Eur. Phys. J. B **39**, 491–498 (2004)
DOI: 10.1140/epjb/e2004-00222-x

THE EUROPEAN PHYSICAL JOURNAL B

Surface plasmon resonance in nanocrystalline silver in a ZnO matrix

R.K. Roy[1], S. Bandyopadhyaya[1,2], and A.K. Pal[1,a]

[1] Department of Materials Science, Indian Association for the Cultivation of Science, Calcutta-700 032, India
[2] St. Xavier's College, 30 Park Street, Calcutta-700 016, India

Received 23 October 2003
Published online 23 July 2004 –

Abstract. Silver nanoparticles embedded in ZnO matrix were deposited onto fused silica substrates using high pressure (∼40 Pa) d.c. sputtering techniques. The particle size in the films was tailored by varying the system pressure and substrate temperature, while the metal volume fraction was controlled by adjusting the relative time of sputtering of the targets. Blue-shift of the surface plasmon resonance peak was observed with the reduction in size and volume fraction of metal particles. A surface plasmon peak in the absorption spectra was found to be absent in the films with particle size and metal concentration below a critical value. A sharp absorption edge in the absorbance spectra within the UV-VIS range indicated semiconducting behavior of the ultrafine silver particles. Films deposited at lower substrate temperature showed a narrow distribution of nanoparticles, nearly spherical in shape. Increase in substrate temperature resulted in a non-uniform size and shape in the films due to the agglomeration of the nanoparticles. These size and shape distributions have a profound effect on the optical absorbance spectra and result in a broad and asymmetric surface plasmon band. A shape distribution introduced in the Maxwell-Garnett or Bruggeman effective medium theory was found to give a reasonable description of the experimentally observed optical absorption spectra.

PACS. 78.67.-n Optical properties of low-dimensional, mesoscopic, and nanoscale materials and structures – 78.67.Bf Nanocrystals and nanoparticles

1 Introduction

Composite films consisting of nanosized metal particles embedded in various matrices show novel physical properties conducive to potential applications in various optoelectronic devices [1–4]. Nanoparticles can be used as the building blocks for photonic or microelectronic devices that possess high frequency signals. Extensive work has now been done on different metal nanocomposite systems. These nanocomposite films exhibit large third order nonlinear susceptibility near the surface plasmon resonance frequency with fast photonic or microelectronic devices that possesses high frequency signals. In recent years there has been considerable interest in investigating surface plasmon resonance of these systems, comprising of silver or gold nanoparticles embedded generally in a SiO_2 dielectric matrix [5–8]. The frequency of the surface plasmon resonance depends on the dielectric properties of the metal and the embedding material [9,10] as well as on the size and shape of the metal nanocrystallites.

Several attempts have been made to date to model the optical absorption spectra by taking into account the effect of size and its distribution [1,11–15]. In contrast, the effect of shape distribution on the optical properties and effective dielectric constant has drawn less attention. The effective medium theory introduced by Maxwell Garnett [16] and Bruggeman [17] considered spherical or ellipsoidal shape of the nanoparticles to model the optical absorption spectra. Later, Gao et al. [18] considered a shape distribution to describe the effective dielectric constant of a two component composite material in which one of the components had a shape (ellipsoidal) distribution. The present study focuses on the dependence of the surface plasmon resonance frequency on size, shape and dielectric properties of the silver nanoparticles embedded in zinc oxide matrix.

2 Experimental

Silver and ZnO targets (99.999%) were sputtered sequentially in argon plasma at a system pressure of ∼40 Pa to deposit Ag/ZnO nanocomposite films. The films were deposited onto fused silica substrates at different substrate temperature and deposition times. The temperature of the substrate, placed on a heavy copper block serving as the substrate holder, could be varied by pouring liquid nitrogen in the dewar attached to the substrate holder and

[a] e-mail: msakp@iacs.res.in

monitored/ controlled by a copper-constant thermocouple through an on/off electronic temperature controller. The targets were pre-sputtered with a shutter located between the target and the substrate before actual deposition was made. Duration of deposition of the individual layers was monitored and controlled by this shutter. The depositions were carried out at 1.5 KV and 50 mA with the target (2.5 cm dia) and substrate distance of ∼2.5 cm. Films were deposited simultaneously under identical deposition conditions onto freshly cleaved NaCl substrates for TEM studies, fused silica and glass for optical and AFM studies. A Hitachi H-600 transmission electron microscope and a Hitachi U-3410 spectrophotometer were used to record the TEM images and optical absorbance respectively. XRD traces were recorded by a Seifert 3000P diffractometer.

3 Results and discussion

Ultra-fine metal particles embedded in dielectric matrix in thin film form are generally characterized by the presence of a very large surface to volume ratio of metal nanocrystallites constituting the film. The size of the crystallites and intercrystallite distance could be modulated by the deposition condition. The intercrystallite distances are determined by the volume fraction of the metal particle loading in the insulating matrix and as such it behaves like a disordered system. Thus, the properties of these systems are different from those in the bulk with long range order and interaction effects play a major role in the electronic properties [5–8] of the granular metal films.

The interaction between the small metal nanocrystallites with the external electromagnetic field induced by light is known to result in a coherent oscillation of the conduction (free) electrons (mainly within the surfaces), called the surface plasmon resonance (SPR). The particle size and shape of the metallic material and its surrounding environment would largely modulate the SPR in these films. During sputtering at a higher pressure than the normal sputtering regime, the particles ejected from the target will undergo numerous collisions with the argon gas atoms. Gas collisions will lower the ejected kinetic energy of the sputtered material and as such will convey less thermal energy to the substrate. Since the kinetic energy of the sputtered silver atom is low compared with that of its latent heat, the release of surface energy will be through the release of latent heat. The silver particles would then subsequently nucleate on the substrate by rapid condensation to form ultrafine particles. The arrival rate of the ejected material could thus be lowered by diffusion losses, by suitably adjusting the input power, and hence one could avoid agglomeration of silver particles on the non-affinitive base (glass/silicon). Thus, it would be possible to deposit a series of films with different grain sizes and inter-grain separations by varying the pressure and substrate temperature during deposition.

The effect of particle size, shape, metallic volume fraction and effective dielectric behavior of the surrounding matrix on the surface plasmon resonance was studied by depositing three sets of silver films embedded into ZnO matrix as above. The films were deposited at substrate temperatures (T_s) ∼ 233 K, 253 K and 273 K respectively. At each T_s, the silver target was sputtered for different durations ranging from 5–180 s, keeping the sputtering time for the ZnO target fixed at ∼360 s such that at each substrate temperature, films with different silver nanocrystallite loading could be obtained. Thus, by sequential sputtering of the silver and ZnO targets and varying substrate temperature (T_s) and deposition time (t), it would be possible to deposit films with different particle size with different metal volume fraction (f) without any major agglomeration occurring in the deposited films. The average thickness of the films was estimated to vary between 5 nm and 20 nm.

Figures 1a–e shows the TEM images, diffraction patterns and the corresponding size distribution of three representative nanocomposite films deposited at $T_s = 253$ K with deposition time (t) ∼150 s (Fig. 1a) and ∼180 s (Fig. 1b) and at $T_s = 273$ K for ∼150 s (Fig. 1c). One may observe a typical increase in silver nanoparticle loading with increase in sputtering time of silver with a narrow distribution of particle size. Effect of grain growth is depicted by the representative micrograph (Fig. 1c) for a film deposited at higher temperature (∼273 K) with sputtering time of silver ∼150 s. Significant grain growth due to increased adatom mobility with the increase in substrate temperature is distinctly visible from the micrographs of the films deposited at $T_s = 253$ K (Fig. 1a) and $T_s = 273$ K (Fig. 1c) when the deposition time was kept constant at $t = 150$ s. The diffraction patterns indicate that films are preferentially oriented and preferred orientation increased as the number density of silver particles increased (Fig. 1c). Figures 1d and e show the lattice resolution picture of the film whose micrograph is shown in Figure 1a. As the sizes of the silver and ZnO nanoparticles are different, it was difficult to focus at the boundary showing simultaneously lattice resolved pictures for both of the materials. Figure 1d shows the lattice resolution picture of silver particles and Figure 1e shows the lattice resolved picture for adjacent ZnO which clearly indicates the existence of preferentially oriented ZnO crystallites. The lattice spacing of nano-Ag obtained from the above micrograph (Fig. 1d) is 0.24 which matches well with that for (111) planes of cubic lattice of the bulk. Figure 1e shows two adjacent ZnO crystallites oriented in (002) and (100) with lattice spacing of 0.28 nm and 0.30 nm respectively. It appears that the lattice is dilated more for ZnO (∼6.5%) than for silver (∼2%).

Figure 2 shows the XRD pattern of a representative film deposited at $T_s = 273$ K with deposition time ∼120 s. The XRD trace is dominated by a strong peak of Ag at $2\theta \sim 38.1°$ for reflections from (111) planes followed by a smaller ones at $2\theta \sim 42.2°$, 64.4° and 77.3° for reflections from (200), (220) and (311) planes respectively. Peaks related to ZnO are also visible at $2\theta \sim 32.4°$, 50°, 59°, 66.9° and 72.4° for reflections from (100), (102), (110), (112) and (004) planes respectively.

The optical absorbance spectra of the nanocomposite films deposited at $T_s = 273$ K, 253 K and 233 K are

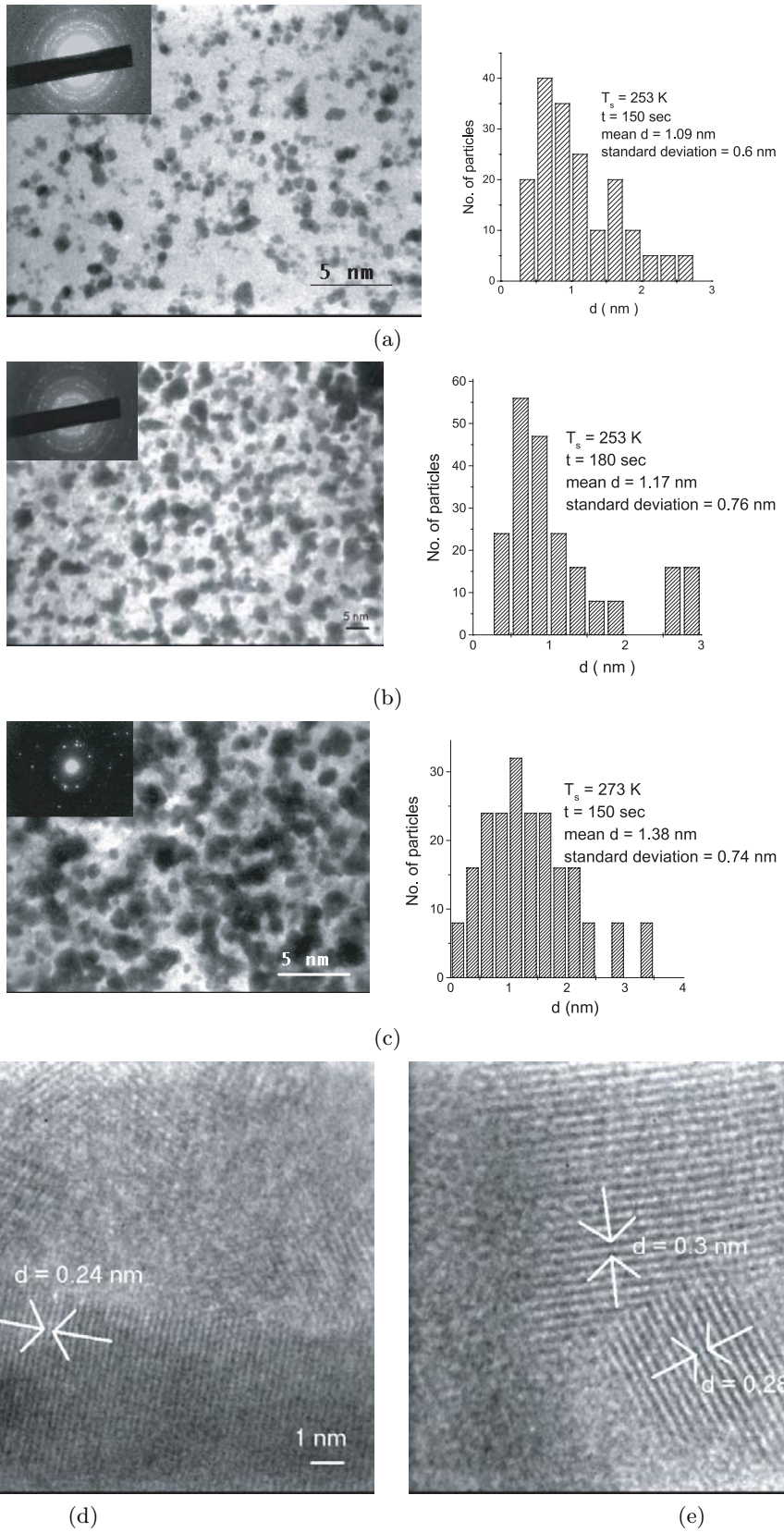

Fig. 1. TEM micrographs along with the particle size distribution of three representative films deposited at $T_s = 253$ K with deposition time: (a) $t = 150$ s and (b) $t = 180$ s and (c) at $T_s = 273$ K with deposition time $t = 150$ s respectively. HRTEM images of a representative film ($T \sim 273$ K; $t \sim 150$ s) showing lattice spacing for: (d) silver and (e) ZnO.

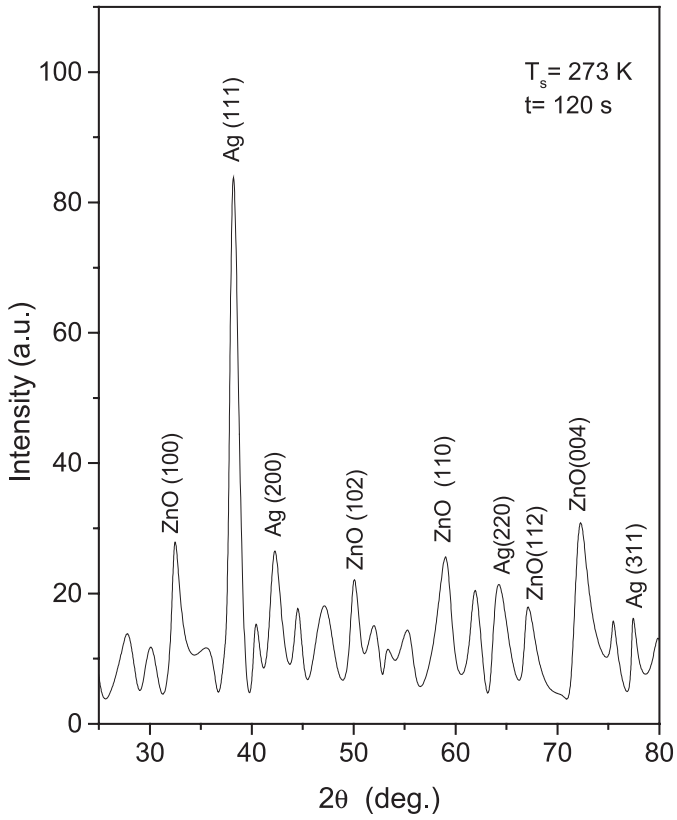

Fig. 2. XRD spectrum of a representative film with $T_s = 273$ K and deposition time 120 s.

shown in Figures 3a–c respectively. Keeping the substrate temperature fixed, the films were deposited at different deposition times as indicated in the above figures. The absorption peaks due to the surface plasmon resonance effect could be seen to be red-shifted with the increase in silver-volume fraction f (i.e. with sputtering time of Ag) for all the three sets of films deposited at three different deposition temperatures. The absorption bands are also broad and become asymmetric with increasing volume fraction of silver nanocrystallites. The observed red shift of the plasmon band is a characteristic feature of the composite films having large volume fraction of silver nanoparticles which may be attributed to the increased electromagnetic interaction between the particles [19,20] and a change in the effective permittivity of the surrounding matrix. The observed shift in the peak position of the surface plasmon bands for films deposited at different T_s but at a fixed time are shown in Figure 4. The surface plasmon peak position could be seen to be blue-shifted with decrease in T_s (i.e. with reduction of particle size). It may be observed (Figs. 1a–d) that the inter-particle, distances became smaller with the increase in number density of silver particles, and the silver nanoparticles still remain isolated from each other. A single absorption peak corresponding to dipolar interaction between the particles dominates the optical absorbance spectra. Thus, presence of higher order multipole interaction among the nanoparticles that would manifest into a splitting of the single absorption peak into

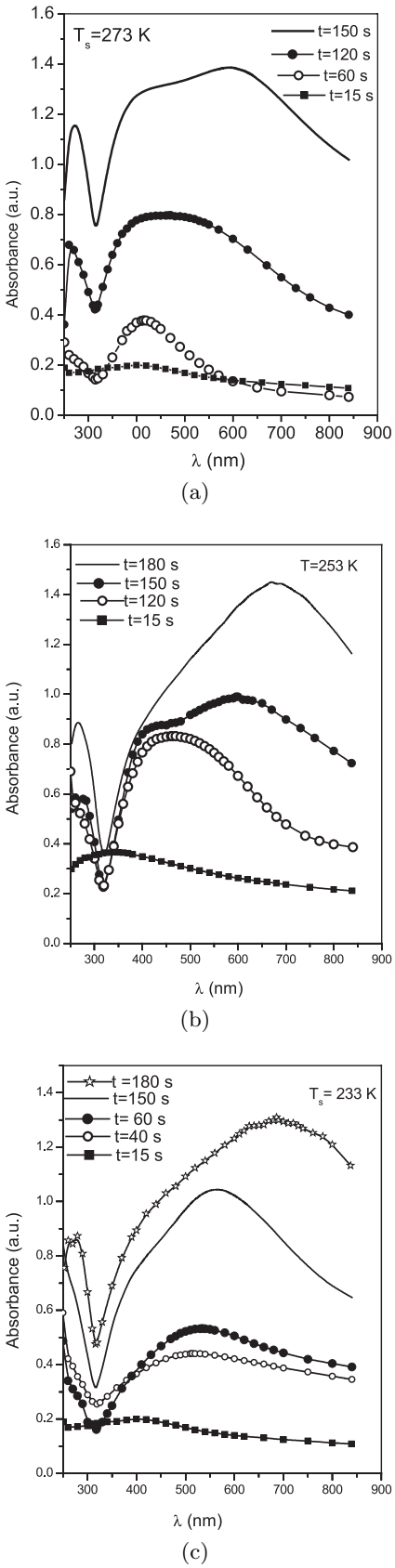

Fig. 3. Optical absorbance spectra of nano-composite silver films deposited at (a) $T_s = 273$ K, (b) $T_s = 253$ K, (c) $T_s = 233$ K with different deposition time respectively.

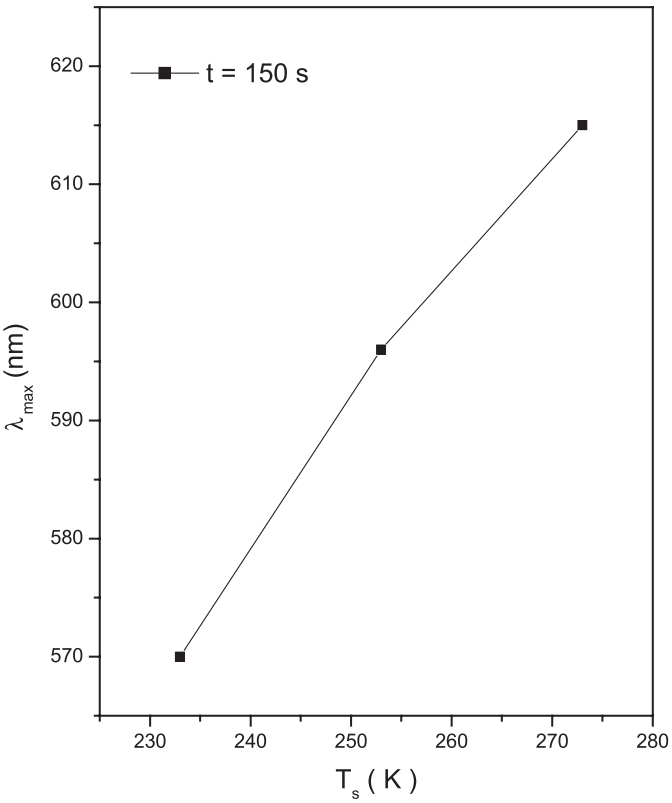

Fig. 4. Variation of surface plasmon resonance peak (λ_{max}) with substrate temperature T_s.

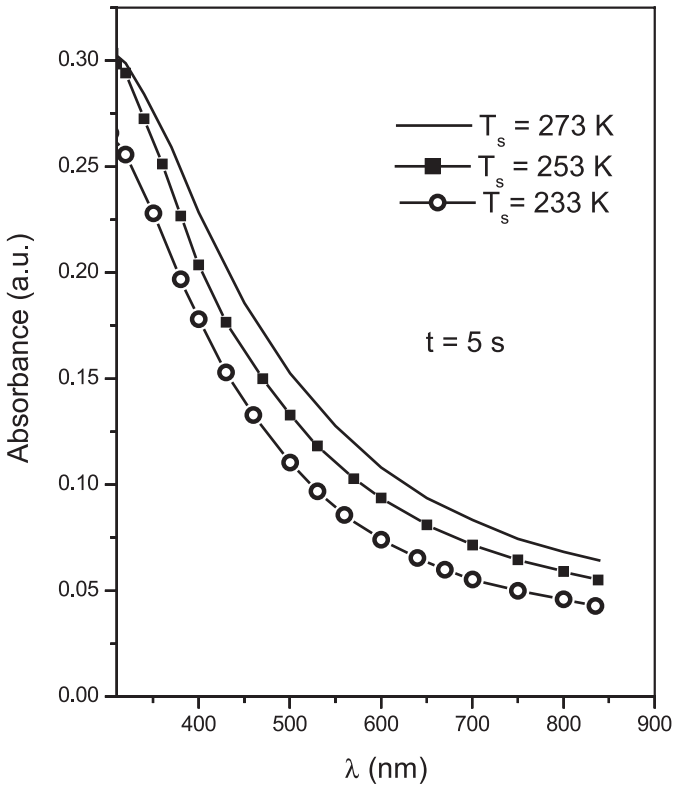

Fig. 5. Optical absorbance spectra of nanocomposite silver films with deposition time 5 s and T_s = 233 K, 253 K, 273 K respectively.

several peaks, and new features in the absorbance spectra could be ruled out [21].

A number of theoretical models were proposed [9,22–30] and experiments were carried out to understand the observed peak shift (either blue-shift or red-shift) and its broadening with decreasing size. The blue-shift was attributed to contraction of the lattice induced by surface stress [29], effect of surface potential [31], changes of optical interband transitions between the discrete energy levels, changes of electron band structure etc. The red shift is regarded as the spill-out of the s-electrons in free electron metal [32], increase in the effective mass of the conduction electrons etc. Besides the above effects, deviation from perfect spherical shape, and irregular size distribution would profoundly effect the large inhomogeneous broadening [33].

It may be observed from Figures 3a–c that when the films are deposited for smaller durations (∼15 s), surface plasmon peaks with low intensity start appearing for all the films deposited at different substrate temperatures. These films have very low metal loading with large intercrystalline distances. Thus, these silver nanocrystallites would behave like isolated nanocrystallites in which, due to the quantum confinement effect, the energy bands would be discrete in nature and the energy levels would be widely spaced. This would result in the reduction in the number of electrons to be transferred to the surface plasmon states and single electron excitations between the quantized energy levels would take place [7]. Thus, instead of the collective oscillation of the electrons, plasmons will be confined to isolated ultrafine grains [34] and will be largely broadened. It may be noticed that with the increase of deposition temperature, the surface plasmon resonance peak in the absorbance spectra became stronger for films deposited at higher substrate temperature. It may also be noted here that films with still lower silver loading (i.e. sputtering time for silver ∼5 s), no surface plasmon peaks were observed for all the films deposited at different substrate temperature. The optical absorbance spectra of these films resembled that of semiconductors (Fig. 5) having a sharp absorption edge with a direct band gap [35]. Also, the absorption edge changed to lower wavelength for films deposited at decreasing substrate temperature from 273 K to 233 K. This would mean that the surface plasmon resonance state would be suppressed giving rise to a sharp absorption edge corresponding to semiconducting optical properties when the nanocrystallite size and metal concentration drop below a critical value. Now, if we look at the plot (Fig. 6) of the first derivative of transmission coefficient (T_r) with wavelength (λ) for the films deposited at different temperatures but at a fixed time $t \sim 5$ s, one can observe that the peaks in the $dT_r/d\lambda$ versus λ spectra are shifted (Fig. 6) to higher wavelength (i.e. lower energy). This peak position would correspond to the band gap (E_g) of the nanocomposite silver films, and the change in band gap with decreasing

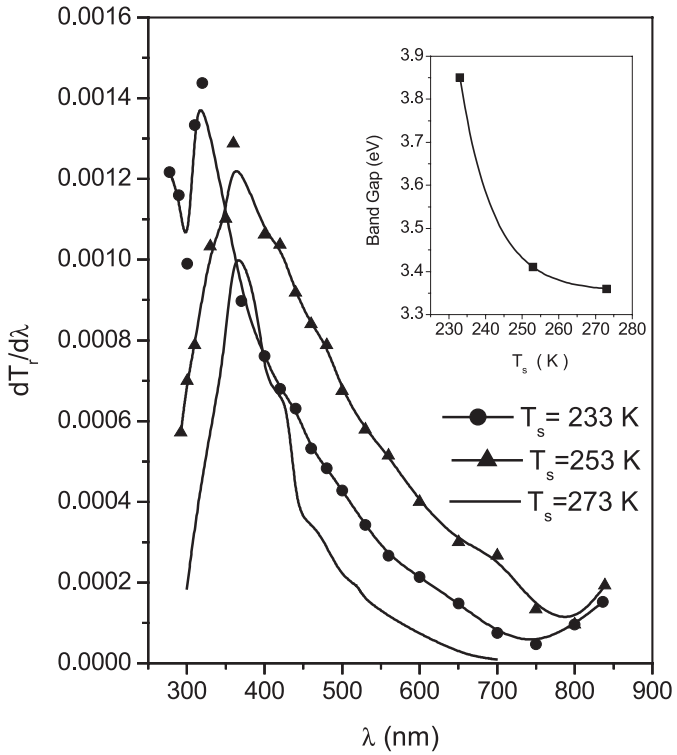

Fig. 6. Plot of $(dT_r/d\lambda)$ with λ for films deposited for 5 s and with T_s = 233 K, 253 K and 273 K respectively. Inset shows the variation of band gap (E_g) with T_s.

deposition temperature (i.e. with decreasing particle size) derived as above indicates blue shift (inset of Fig. 6).

It may be noted here that the optical extinction spectra of these systems were found to be described well by Mie's theory [1,11,36]. The Mie theory generally accounts well for the size of the isolated metal particles in the optical spectra but is restricted to spherical shape only. It was observed that the plasmon-derived resonance of silver nanocrystallites became stronger and broader as the volume fraction of silver nanocrystallites increased. The resonance peak also shifted towards higher wavelength with the increase in the loading of silver nanocrystals in ZnO matrix. This behaviour is in agreement with the TEM observation and indicates that the size of the nanocrystallites increases, and the size-distribution of the nanocrystallites broadens, with the increase in loading of silver crystallites. It may be interesting to see how the optical absorbance behavior of these composite films could be represented by the effective medium theory predicted by Maxwell-Garnett [16,37,38]. The MG theory is strictly valid in the limit of $d/\lambda < 0.1$ along with very small interparticle distances for spherical particles. According to the MG theory the effective complex dielectric constant ε_c for a composite system containing spherical metal particles embedded in a host matrix is defined by:

$$\varepsilon_c = \varepsilon_0 \frac{\varepsilon_m(1+2f) + 2\varepsilon_0(1-f)}{\varepsilon_m(1-f) + \varepsilon_0(2+f)}. \quad (1)$$

The complex dielectric constant ε_c is related to the refractive index n_c and absorption coefficient k_c via the following equations:

$$\varepsilon_c = n_c^2 = \varepsilon_{c''} + i\varepsilon_{c'} \quad (2)$$

$$\varepsilon_{c'} = n_c^2 - k_c^2 \text{ and } \varepsilon_{c''} = 2n_c k_c. \quad (3)$$

The absorption maximum occurs at wavelength that satisfies the following relation:

$$(1-f)\varepsilon_1 + (2+f)\varepsilon_0 = 0. \quad (4)$$

From Figures 3a–c it is clear that there exists a red shift with increasing loading of silver which in turn increases the f. But the simulated surface plasmon resonance maximum obtained through equations (1–4) cannot explain these properly. The experimental spectra are not symmetric about the maximum which cannot be represented by the spherical grain approximation in original M-G theory. Thus, the M-G model appears to be inadequate to represent the optical absorbance with particles of different size and nonspherical shape. The modified theory called the dynamical MG (DMG) theory [38,39] is supposed to take into account the finite size and shape of the particles and the result obtained in the light of this DMG theory is described below.

To study the effect of particle shape on the surface plasmon resonance in these films, we have selected a representative film deposited at higher substrate temperature (whose micrograph is shown in Fig. 1) when the shape of the nanocrystallites deviated significantly from spherical nature due to enhanced adatom mobility resulting in coalescence of the adjacent nanocrystallites. The films deposited at higher T_s indicated a broad distribution of size and shape (prolate) due to the coalescence of the adjacent nanoparticles. This would give rise to an anisotropic mixture of the metal nanoparticles and insulating matrix. To take into account the size as well as the shape simultaneously, a size dependent depolarization factor was introduced by Gao et al. [18] into the Maxwell-Garnett theory and the modified theory (dynamical Maxwell-Garnett theory) was used to evaluate the optical properties of the gold nanocomposite material [39]. The depolarization factor played a crucial role in determining the optical absorption features.

Assuming the particles to be ellipsoidal, a distribution function $P(L)$ was introduced to rationalize the theoretical description of the depolarization coefficient:

$$P(L) = \frac{A}{\sqrt{L(1-L)}} \quad (5)$$

where A $(= 1/\pi)$ and L $(0 < L < 1)$ are the normalization constant and equivalent depolarization factor respectively. The two extreme values of L i.e. $L \to 0$ and $L \to 1$ determine a needle-like (prolate) and plate-like (oblate) shape of the particles. The depolarization factor depends critically on the axial ratio of the ellipsoidal particles [39,40]. Thus, Gao et al. [18] obtained the dielectric constant in

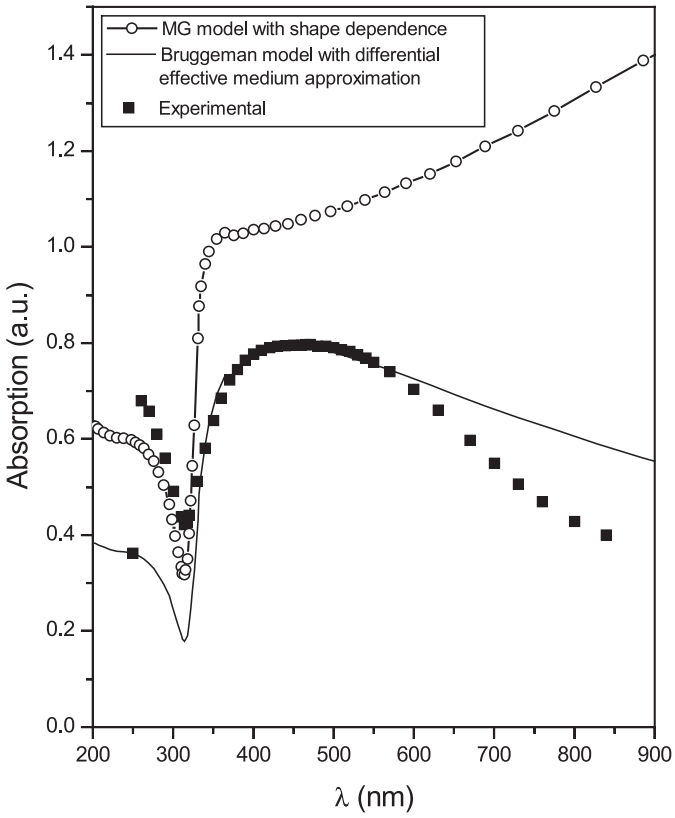

Fig. 7. Fit of experimental absorbance spectra simulated from equation (7).

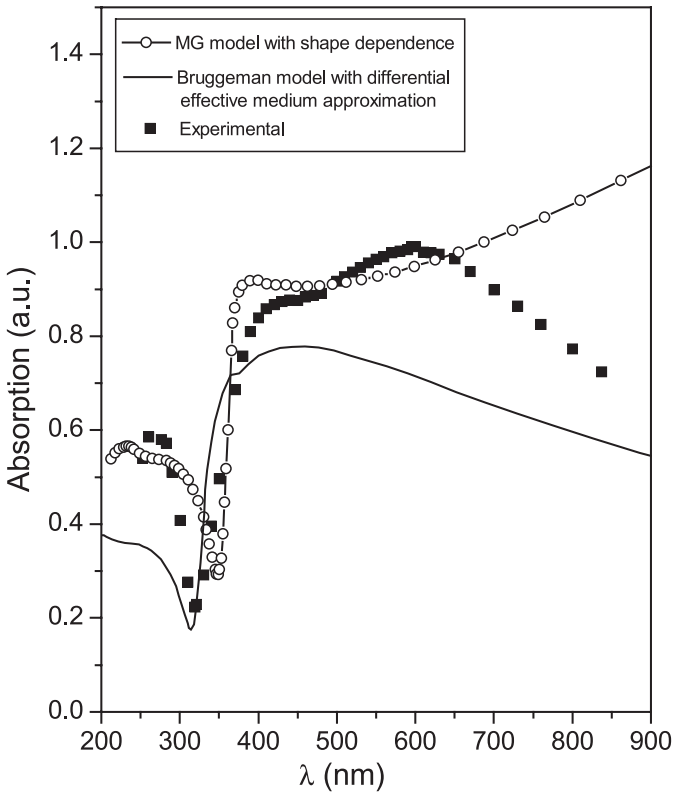

Fig. 8. Fit of experimental absorbance spectra simulated from equation (6).

the limit of Maxwell-Garnett approximation as:

$$\frac{\varepsilon_c}{\varepsilon_o} = \frac{1 + f(\sqrt{\varepsilon_m/\varepsilon_o} - 1)}{1 + f(\sqrt{\varepsilon_o/\varepsilon_m} - 1)}. \quad (6)$$

The differential effective medium approximation along with shape dependence in Bruggeman type homogeneous matrix, was formulated as:

$$\frac{\varepsilon_c}{\varepsilon_o} = \frac{1 + f + (1 - f)\sqrt{\frac{\varepsilon_m}{\varepsilon_o}}}{1 - f + (1 + f)\sqrt{\frac{\varepsilon_m}{\varepsilon_o}}}. \quad (7)$$

Now, taking into account the shape distribution, the absorbance spectra were computed by using equation (7) based on the Bruggeman modified model. Here, the shape of the particles is considered to be ellipsoidal having a distribution as indicated in equation (5). Figure 7 shows the simulated absorption spectrum of a representative film (deposited at 273 K for 120 s) having nearly similar prolate crystallites shown in Figure 1c. One can easily observe that the simulated absorption spectrum (Fig. 7) obtained from equation (7), i.e. the differential Bruggeman-type of effective medium approximation describes the experimental absorbance spectra more faithfully. The inhomogeneous broadening due to fluctuation in shape is considered well with this approximation. It may be noted here that the fit of the experimental data with equation (6) is still quite poor in the higher wavelength region (Fig. 7). Nevertheless, incorporation of the shape distribution in our nanocomposite films was found to be more effective to enable interpretation of the experimental observations for optical absorption. It is interesting to observe the comparison between the experimental and simulated absorption spectra (Fig. 8) for a film (whose micrograph is shown in Fig. 1a) having nearly isolated spherical silver nanocrystallites. The Maxwell-Garnett model seemed to describe the experimental data more faithfully than that of the Bruggemann modified model which considered elliptical nanocrystallites. Thus, it is quite clear that the shape of the nanocrystallites would modulate the surface plasmon resonance in these systems.

It is necessary to mention here that as well as particle size and shape, the surrounding matrix/support (i.e. ZnO) will also influence the energy as well as the width of the surface plasmon resonance [7,30,41]. In computing the absorbance spectra, it was assumed that nanosized Ag and ZnO had the same value for the dielectric constants as their bulk. Also, dipole–dipole interaction was only considered while one may not rule out quadrupole and higher multipole interactions between nanoparticles in this system. The discrepancy in the higher wavelength region may also be ascribed to that fact that light scattering from larger particles would predominate over the light absorption at the higher wavelength [42]. In fact, the metal-support interaction introduces a shift in the energy of the metal valence orbitals and thereby changes the

electron density of the metal nanoparticles which in turn would modify the electronic properties of the nanoparticles. The local change in the electronic density does affect the effective dielectric constant of the supported metal nanoparticles, and hence their optical absorbance profile. This interaction is also critically dependent on the chemical nature of the supported matrix and associated chemical interface effects associated with it. Hövel et al. [30] have described how the chemical interface damping arising out of the chemical properties of the interface, and energy transfer between cluster and the support by temporary charge transfer reactions, can alter the plasmon resonance of the supported metal nanoparticles. Mojet et al. [41] also demonstrated the effect of the chemical nature of the support on the spectroscopic and catalytic properties of the noble metal catalysts.

4 Conclusions

Nanocomposite silver films of various volume fractions with a very narrow size distribution of particles were prepared by high pressure sputtering techniques. The optical absorption peak corresponding to the surface plasmon resonance showed a red shift with increasing particle volume fraction but blue shifted with the decrease in particle size. However when the particle size and volume were reduced to a critical value, the surface plasmon band was suppressed and instead showed a sharp absorption feature corresponding to semiconducting properties with a direct band gap. Surface plasmon resonance spectra were also simulated by Mie theory, and Maxwell-Garnett effective medium theory. The film containing a distribution of particle size and shape results into an inhomogeneously broadened surface plasmon resonance in the optical absorption spectra. A simple M-G or Bruggeman approach considering the spherical shape of the nanoparticles could not faithfully represent the experimentally observed surface plasmon resonance in films in which shape of the nanocrystallites deviated from spherical nature. Consideration of particle shape distribution accounted for the inhomogeneous broadening of the plasmon band of the nanocomposite films.

We wish to thank Mr. B. Satpati, Institute of Physics, Bhubaneswar, India for his support in recording the TEM micrographs. One of the authors (R.K. Roy) wishes to thank the Council of Scientific and Industrial Research (CSIR), Government of India, for extending junior research fellowship in carrying out this programme.

References

1. U. Kreibig, M. Vollmer, *Optical Properties of Metal Clusters* (Springer, New York, 1995)
2. K. Uchida, S. Kaneko, S. Omi, C. Hata, H. Tanji, A. Asahara, A.J. Ikushma, T. Tokizaki, A. Nakamura, J. Opt. Soc. Am. B **11**, 1236 (1994)
3. J.H. Shin, G.N. van den Hoven, A. Polman, Appl. Phys. Lett. **66**, 2379 (1995)
4. M. Fujji, M. Yoshida, Y. Kanazawa, S. Hayashi, K. Yamamoto, Appl. Phys. Lett. **71**, 1198 (1997)
5. Z. Liu, H. Wang, H. Liu, X. Wang, Appl. Phys. Lett. **72**, 1823 (1998)
6. R. Antoine, M. Pellarin, B. Palpant, M. Broyer, B. Prevel, P. Galletto, P.F. Brevet, H.H. Girault, J. Appl. Phys. **84**, 4532 (1998)
7. L. Yang, G. Li, L. Zhang, Appl. Phys. Lett. **76**, 1537 (2000)
8. J.R. Jackson, N.J. Halas, J. Phys. Chem. B **105**, 2743 (2001)
9. U. Kreibig, L. Genzel, Surf. Sci. **156**, 678 (1985)
10. T. Klar, M. Perner, S. Grosse, G. von Plessen, W. Spirkl, J. Feldmann, Phys. Rev. Lett. **80**, 4249 (1998)
11. G. Mie, Annl. Phys. **25**, 377 (1908)
12. R. Jenson Traci, C. Schatz George, P. Van Duyne Richard, J. Phys. Chem. **103**, 2394 (1999)
13. A. Foss Colby Jr, J. Tierney Michael, R. Martin Charles, J. Phys. Chem. **96**, 9001 (1992)
14. W.P. Barber, K.R. Chang, H. Massoudi, Phys. Rev. B. **27**, 7251 (1983)
15. S.K. Mandal, R.K. Roy, A.K. Pal, J. Phys. D. **36**, 261 (2003)
16. J.C. Maxwell-Garnett, Philos. Trans. R. Soc. London A **203**, 385 (1904)
17. G.A.D. Bruggeman, Ann. Phys. Lpz. **24**, 636 (1935)
18. L. Gao, J.Z. Gu, J. Phys. D. **35**, 267 (2002)
19. Claro Fransisco, Phys. Rev. B **25**, 7875 (1982)
20. L. Genzel, T.P. Martin, Surf. Sci. **34**, 33 (1973)
21. N. Stefanou, A. Modnos, 1991 J. Phys.: Condens, Matter **3**, 8149 (1991)
22. B.N. Persson, A. Liebsch, Phys. Rev. B **28**, 4247 (1983)
23. D. Bedeaux, J. Vleger, Thin Solid Films **102**, 265 (1983)
24. S. Fedrigo, W. Harbich, J. Buttet, Phys. Rev. B **47**, 10706 (1993)
25. K. Arisato, K. Ryogo, J. Phys. Soc. Jpn **21**, 1765 (1996)
26. V.V. Kresin, Phys. Rev. B **51**, 1884 (1995)
27. H.W. Chu, T. Juh, Phys. Rev. B **49**, 17279 (1994)
28. J. Larme, B. Palpant, B. Prevel, M. Pellarn, M. Trielleux, J.L.Vialle, A. Perez, Broyer M. Broyer, Phys. Rev. Lett. **80**, 5105 (1998)
29. W. Cai, H. Hofmeister, M. Dubiel, Eur. Phys. J. D **13**, 245 (2001)
30. H. Hövel, S. Fritz, A. Hlger, U. Kreibig, Phys. Rev. B **48**, 18178 (1993)
31. F. Cocchini, F. Bassani, Surf. Sci. **156**, 851 (1985)
32. W.A. de Heer, Rev. Mod. Phys. **65**, 611 (1993)
33. R. Gans, Ann. Physik **37**, 881 (1912)
34. F. Moresco, M. Rocca, T. Hildebrandt, M. Henzler, Phys. Rev. Lett. **83**, 2238 (1999)
35. W. Cai, Z. Ye, J. Junhui, Zhang Lide, Appl. Phys. Lett. **73**, 2709 (1998)
36. G.W. Arnold, J.A. Borders, J. Appl. Phys. **48**, 1488 (1977)
37. L. Hornyak Gabor, J. Patriss Charles, R. Martin Charles, J. Phys. Chem. B **101**, 1548 (1997)
38. C.A. Foss Jr, G.L. Hornyak, J.A. Stockert, C.R. Martin, J. Phys. Chem. **96**, 7479 (1992)
39. C.A. Foss Jr, G.L. Hornyak, J.A. Stockert, C.R. Martin, J. Phys. Chem. **98**, 2963 (1994)
40. C.G. Granqvist, O. Hunderi, Phys. Rev. B **16**, 3513 (1977)
41. B.L. Mojet, J.T. Miller, D.E. Ramaker, D.C. Koningsberger, J. Catalysis **186**, 373 (1999)
42. C.R. Bamford, *Glass Science and Technology*, Vol. 2 (Elsevier, Amsterdam, 1977)